NANO LETTERS

Letter

pubs.acs.org/NanoLett

Interplay of Wrinkles, Strain, and Lattice Parameter in Graphene on Iridium

Hichem Hattab,[†] Alpha T. N'Diaye,[‡,⊥] Dirk Wall,[†] Claudius Klein,[†] Giriraj Jnawali,[†,¶] Johann Coraux,[§] Carsten Busse,[‡] Raoul van Gastel,[∥] Bene Poelsema,[∥] Thomas Michely,[‡] Frank-J. Meyer zu Heringdorf,[†] and Michael Horn-von Hoegen*[,†]

[†]Department of Physics and Center for Nanointegration Duisburg-Essen (CeNIDE), University of Duisburg-Essen, Lotharstrasse 1, 47057 Duisburg, Germany

[‡]Department of Physics, University of Cologne, Zülpicher Strasse 77, 50937 Cologne, Germany

[§]Institut NÉEL, CNRS & Université Joseph Fourier, BP166, F-38042 Grenoble Cedex 9, France

[∥]Physics of Interfaces and Nanomaterials, MESA+ Institute for Nanotechnology, University of Twente, P.O. Box 217, NL-7500AE Enschede, The Netherlands

ABSTRACT: Following graphene growth by thermal decomposition of ethylene on Ir(111) at high temperatures we analyzed the strain state and the wrinkle formation kinetics as function of temperature. Using the moiré spot separation in a low energy electron diffraction pattern as a magnifying mechanism for the difference in the lattice parameters between Ir and graphene, we achieved an unrivaled relative precision of ±0.1 pm for the graphene lattice parameter. Our data reveals a characteristic hysteresis of the graphene lattice parameter that is explained by the interplay of reversible wrinkle formation and film strain. We show that graphene on Ir(111) always exhibits residual compressive strain at room temperature. Our results provide important guidelines for strategies to avoid wrinkling.

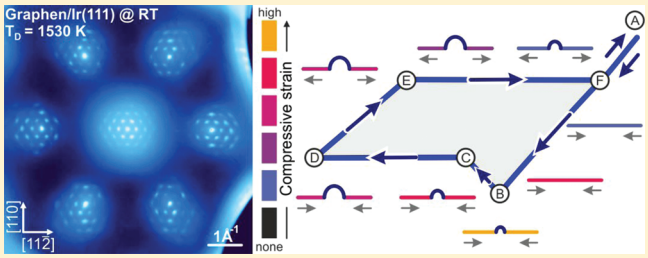

KEYWORDS: *Graphene, strain state, wrinkle formation, LEED, iridium*

Graphene has been suggested as a material for a number of applications, including radio frequency electronics[1,2] high-speed applications,[3] and transparent conductive electrodes.[4]

This potential has created a tremendous research effort to grow graphene layers and to characterize their morphological and electronic properties. Epitaxial growth of graphene on SiC,[5−7] on single-crystalline thin films,[8−12] or on substrates like Ru[13−15] and Ir[16,17] single crystals is well suited in producing large-area graphene, virtually without grain boundaries.[18,19] Graphene growth, however, usually takes place at high temperatures, while any device operation will be performed close to room temperature. This implies that graphene layers on a hot substrate have to be cooled down to room temperature. Because of the mismatch in the thermal expansion coefficients of graphene and the substrate, the graphene layers become compressively stressed during cooling. Ultimately, graphene locally delaminates and forms one-dimensional defects ("wrinkles"). Such wrinkles are encountered in all epitaxial graphene samples.[17,20−25] They have been argued to limit the thermal[26] and electric[27] conductivities, as well as the inertness[28] of graphene. Obviously, a thorough understanding of wrinkle formation and the associated effects is mandatory.

In our previous work, we investigated the formation dynamics of wrinkles using surface microscopy.[23] We found a sudden formation of individual wrinkles during cooling, while these wrinkles were stretched out gradually during heating. In a simple mechanistic model, we proposed an energy barrier for the wrinkle formation and concluded that the graphene between the wrinkles would have to remain compressed at room temperature. Here, we report a hysteresis between formation and disappearance of the wrinkles and present a precise and quantitative in situ analysis of the temperature dependence of the graphene lattice parameter on Ir(111) with high-resolution electron diffraction during cooling and heating of the substrate.

The experiments were performed in an ultrahigh vacuum (UHV) chemical vapor deposition (CVD) reactor with a base pressure of 1×10^{-10} mbar. The system was equipped with a spot profile analysis low energy electron diffraction (SPA-LEED) instrument.[29−31] Spot positions in reciprocal space were determined by fitting Voigt functions to high-resolution SPA-LEED profiles. Furthermore, nonlinearities of the electron optical system of the SPA-LEED were corrected by using the constant separation of the moiré spots at different positions of the diffraction pattern. This advanced analysis reduces the

Received: October 7, 2011
Revised: November 30, 2011
Published: December 16, 2011

   dx.doi.org/10.1021/nl203530t | *Nano Lett.* 2012, 12, 678−682

systematic error and provides us with an increased accuracy for the determination of lattice parameters of ~ ± 0.001 Å. The sample preparation was similar to the one in our earlier studies of graphene growth.[18,19,32] A low-miscut Ir(111) sample (Mateck GmbH) was cleaned by repeated cycles of Ar ion sputtering at 1350 K and subsequent annealing to 1600 K until the characteristic (1 × 1) LEED pattern of the bare Ir surface was observed. Samples were mounted in a sample holder (ELMITEC Elektronenmikroskopie GmbH) and heating was performed with electron beam bombardment to the back of the Ir crystal, with the Ir at ground potential. Temperatures were calibrated using an infrared pyrometer.

Graphene was formed by the thermal decomposition of ethylene at elevated temperatures (>1400 K) and an ethylene background pressure of 5×10^{-6} mbar. The decomposition dynamics is self-limiting to a single layer of graphene,[33] and under our conditions the surface is completely covered after less than one minute of deposition.

After formation of graphene, the sample was cooled down to room temperature for characterization of the morphology of the graphene with SPA-LEED. Figure 1a shows a LEED pattern of a graphene layer on Ir, recorded at room temperature. We explain the LEED pattern by double diffraction of electrons at the closed graphene layer and the iridium substrate below.[18] LEED displays characteristic moiré spots surrounding the integer order spots at positions $\vec{G}_{Ir}$ of the Ir reciprocal lattice. We only observe the R0° phase of graphene and there are no rotational graphene domains. The graphene is aligned with the Ir lattice, that is, $\vec{G}_{Ir} \| \vec{G}_{gr}$. Thus, we can apply the 1D moiré condition[34] $k_{moiré} = G_{gr} - G_{Ir}$ to determine the graphene lattice parameter $a_{gr}(T)$ from the temperature dependent Ir lattice parameter $a_{Ir}(T)$. We use temperature-dependent values for the Ir lattice parameter,[35] since the moiré effect acts like a magnifying mechanism for lattice constant differences (~×10), while the direct determination of the absolute Ir or graphene lattice parameter would only be possible with insufficient accuracy. By measuring the moiré spot separation $k_{moiré}$ from 1D LEED profiles in $[11\bar{2}]$ direction as shown in Figure 1b we then obtain

$$a_{gr}(T) = \left(\frac{1}{a_{Ir}(T)} + \frac{\sqrt{3}}{4\pi} k_{moiré}(T) \right)^{-1} \quad (1)$$

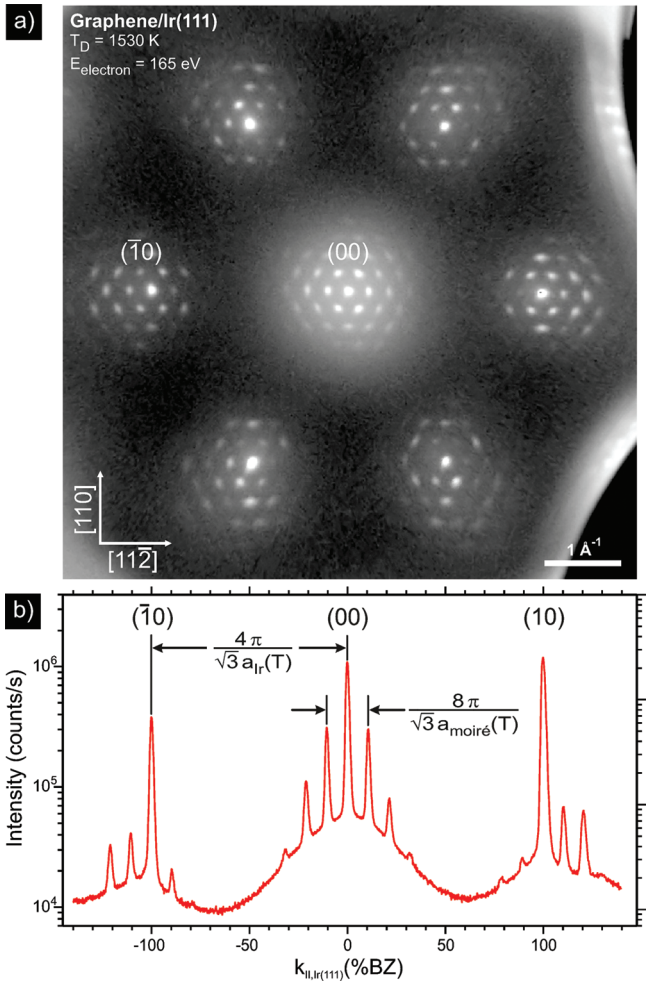

Figure 1. (a) SPA-LEED pattern obtained at RT after graphene growth, displayed in a logarithmic intensity scale. All Ir integer order spots are surrounded by a network of moiré spots. (b) One-dimensional LEED intensity profile along the $[11\bar{2}]$ direction. Ir integer order spots are indicated. The graphene lattice parameter is determined from the separation of the moiré spots.

After sample characterization, we reheated the sample to the growth temperature and allowed some time (~1 h) for thermalization. The sample temperature was then lowered in small steps down to 600 K while recording 1D spot profiles at each temperature step to determine $k_{moiré}(T)$. The data point at room temperature was measured after switching the heating off and allowing the sample to thermalize for ~12 h. The sample was then gradually heated again, and a second set of 1D profiles was recorded.

The measured values for $k_{moiré}$ are shown in Figure 2a, where blue downward triangles originate from the LEED profiles recorded during cooldown and the red upward triangles originate from the LEED profiles recorded during heating. Obviously, the curves recorded during cooling and during heating only coincide at room temperature and at temperatures above 1200 K. The origin of the significant data scatter at high temperatures becomes evident from the insets in Figure 2a, where SPA-LEED profiles through the specular LEED spot are shown at two selected temperatures. At 300 K strong moiré spots are clearly visible, while at 1232 K the Debye–Waller effect causes a poor signal-to-noise ratio.

Figure 2b shows a more detailed analysis by calculating the graphene lattice parameter $a_{gr}(T)$ from the experimentally accessible number for $k_{moiré}(T)$ according to eq 1. The green solid curve shows the aforementioned temperature dependent lattice parameter $a_{Ir}(T)$ for Ir from the literature[36,37] with the scale on the right abscissa. The graphene lattice parameter $a_{gr}(T)$ is plotted for the case of cooling down (blue) and heating up (red) with the scale on the left abscissa. The left abscissa is scaled with respect to the right abscissa so that the lattice parameters of Ir and graphene are found at the same vertical position at room temperature. In this way the deviation of the values from the ones at growth temperature, marker "A", is quantified by the relative change $\varepsilon = (a_0(T) - a_0(A))/a_0(A)$ of the lattice parameter (either thermally induced changes or compression/expansion). Accordingly, an additional abscissa for ε is given on the left which applies to both $a_{Ir}(T)$ and $a_{gr}(T)$. The green dashed curves are shifted parallel to the curve for $a_{Ir}(T)$, shifted by $\varepsilon = -0.25\%$ and $\varepsilon = -0.55\%$ respectively. Our experiment starts at high temperatures at marker A, where the graphene lattice parameter $a_{gr}(T)$ coincides with the almost

dx.doi.org/10.1021/nl203530t | Nano Lett. 2012, 12, 678–682

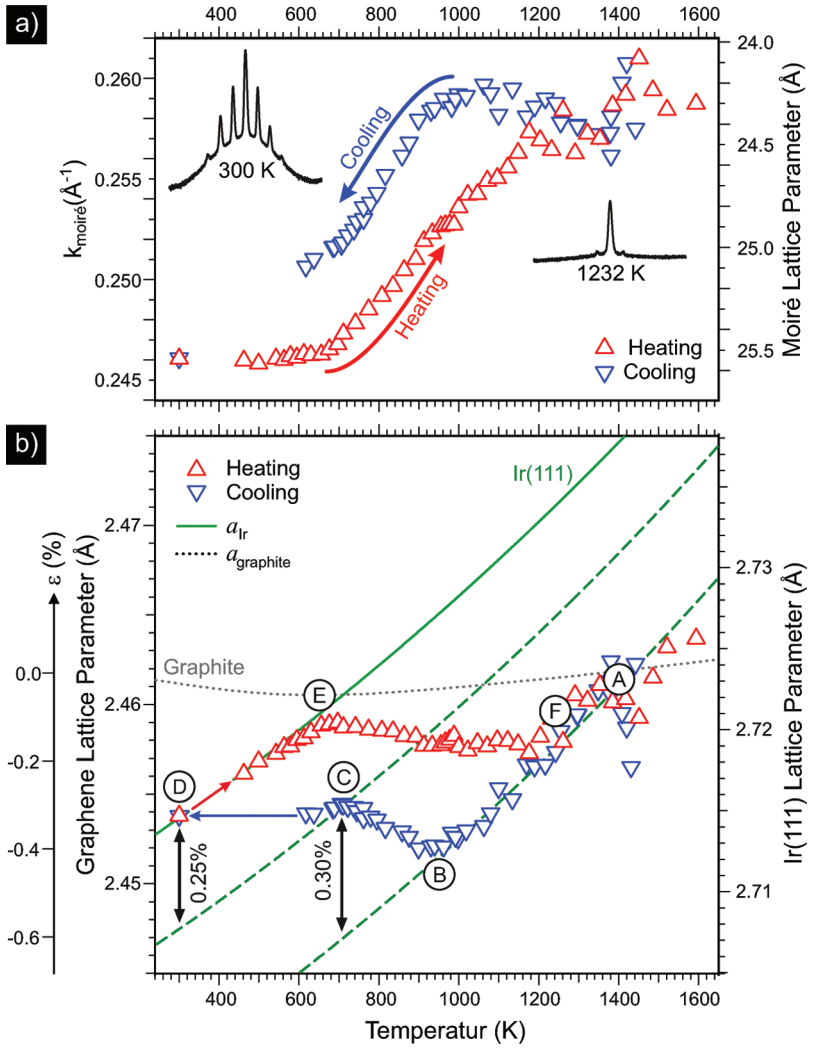

Figure 2. (a) Separation of moiré spots as function of temperature during a cooling and heating cycle. The right abscissa gives the real space periodicity of the moiré pattern. Spot profiles are shown as insets for 300 and 1232 K. (b) The graphene lattice parameter $a_{gr}(T)$ clearly exhibits a hysteresis during the cooling−heating cycle. The Ir lattice parameter is shown as green solid line. Dashed green lines are shifted Ir curves and serve as reference for the temperature dependent behavior. The graphite lattice parameter is shown as a dotted gray line.

temperature independent graphite lattice parameter $a_{graphite}(T)$ taken from literature[38] (dotted gray line). Apparently, graphene grows with the graphite lattice parameter. During cooling by ΔT = 450 K (marker "B") the iridium shrinks thermally by $\varepsilon_{A\rightarrow B}$ = 0.36%. As the graphene data points between A and B fall on the shifted Ir curve, the relative change in lattice parameter of the graphene and the iridium lattice are identical. At marker B we find $a_{gr}(960\ K)$ = 2.452 Å as a global minimum. Surprisingly, upon further cooling by ΔT = 250 K from marker B to marker C, the graphene lattice parameter increases by a value of Δa_{gr} = ∼0.002 Å while the Ir continues shrinking. This small increase is nevertheless significant, since it occurs over a comparatively small temperature range and the change of the Ir lattice parameter is of the same order. After cooling to room temperature (marker D) we find the graphene lattice parameter to be unchanged with respect to marker C while the Ir has shrunk by an additional ε = −0.25%.

If the sample is heated up again, the behavior of the graphene is different from the behavior during cooling. Initially, while heating from room temperature to marker "E" at T = 650 K, the graphene lattice parameter closely follows the expansion of Ir. Further annealing up to marker "F" at T = 1200 K finds the graphene almost unchanged with $a_{gr}(T_{650\rightarrow 1200\ K})$ = 2.458 Å. The slight buildup of compressive strain between E and F should not be over interpreted, as slight systematic errors in the temperature measurement would correspond to a shear operation on Figure 2b and would as such change the small negative slope of the curve between markers E and F. The nature of the observed hysteresis effect, however, and the enclosed area, are not affected. Finally, during annealing above T = 1200 K, the graphene follows the iridium expansion again.

At some temperatures, the graphene lattice parameter simply scales with the thermal expansion of the Ir and builds up or relieves strain, while in the intermediate temperature range, we find deviating behavior. Apparently, a strain relief mechanism exists for the graphene that enables the graphene to relax some of its compressive strain. Moreover, the behavior during cooling is different from the behavior during heating. Such hysteresis indicates the presence of an activated relief mechanism.

The known phenomenon of wrinkle formation[23] in graphene on metals is well suited to explain the observed behavior as sketched in Figure 3. During cooling from marker A to marker B the graphene film builds up a large amount of compressive strain of ε = −0.36% that leaves the graphene in a metastable

dx.doi.org/10.1021/nl203530t | Nano Lett. 2012, 12, 678−682

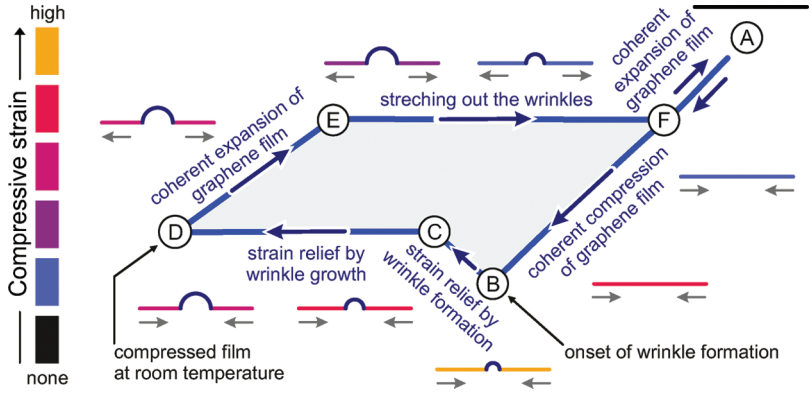

Figure 3. Sketch of the interplay of strain and wrinkle formation of single layer graphene on Ir(111) during a cycle of cooling and heating (blue line and blue arrows). The gray arrows indicate the compression/expansion in the graphene as induced by the thermal expansion/compression of the Ir substrate.

state. At marker B, the strain energy has become large enough to overcome the activation energy for wrinkle formation, and accordingly, the graphene starts to locally relax by forming wrinkles. The finding that the onset of wrinkle formation (B) is approximately 450 K below A agrees well with earlier observations, where wrinkling has been found after a cooldown of 410 K $\pm$ 40 K, independent of the graphene growth temperature.[23] Between markers B and C, the graphene lattice continues to relax into wrinkles, while it remains compressed with a remaining compressive strain of $\varepsilon = -0.3\%$ compared to the graphite lattice constant at the same temperature. Assuming that the energy barrier for wrinkle formation is at least as high as the difference in strain energy before and after wrinkle formation, and using the model from ref 23 we arrive at a lower limit for the energy barrier of $E = 1$ eV/nm. Considering the predicted upper limit for the energy barrier of 2.8 eV/nm,[23] this is a good agreement. We can only speculate whether new wrinkles are formed between markers B and C or whether the strain relief is accomplished by the widening of existing wrinkles. However, the strain needed to form the first wrinkles at marker B is larger than the remaining strain at marker C, which is a hint that indeed for our experiment with a cooling rate of 1 K/min, existing wrinkles become larger. Additional compressive strain induced by the shrinking Ir is immediately relieved by forming or enlarging wrinkles, so that the overall strain in the layer between markers C and D remains constant. In such case not only the formation but also the widening of wrinkles is linked to an activation barrier.

During the entire cooling cycle from marker A to marker D, the Ir lattice parameter has changed by $\varepsilon_{Ir} = -0.88\%$ while the total change of a_{gr} is only $\varepsilon_{gr} = -0.33\%$. The wrinkles accommodate $\varepsilon_{wrinkle} = 0.55\%$ of the strain, that is, ~2/3 of the compressive strain are compensated by wrinkles, while ~1/3 of the compressive strain remains in the graphene layer.

During heating, the Ir expands and the remaining compressive strain of the unwrinkled parts of the graphene layer can be simply relieved when the graphene expands with the Ir lattice. No bond breaking or gliding is required, and the wrinkles stay intact. If instead the graphene lattice parameter followed the Ir lattice parameter beyond marker E, the graphene film would experience buildup of tensile stress. But the graphene lattice parameter remains almost constant beyond marker E, while the wrinkles are stretched out and disappear. Only at temperatures above the one at marker F, after all wrinkles have disappeared, the graphene film is stretched out by the still expanding Ir lattice; with temperatures above the graphene formation temperature the graphene layer is increasingly under tensile stress.

The interplay of strain and wrinkle formation is also reflected in the behavior of the full width at half-maximum (FWHM) of the graphene diffraction spots during the cooling and heating cycle. At high temperatures, when the film is homogeneously strained, the FWHM is constant and resembles the instrumental resolution. During cooling, at temperatures below the one at marker E the FWHM increases due to the incoherent superposition of LEED spots from areas with different strain states, that is, areas close to and further away from wrinkles.

Our data suggests that graphene domains on Ir somehow behave like a (wet) tablecloth that is pinned to the edges of a table. If the tablecloth is pushed in from the sides (by a shrinking table) the cloth will glide, but it will build up strain that is accommodated by compression of the meshes within the fabric. At some point wrinkles will form to partly relax the strain. In the case of the tablecloth there is none, or very little, activation energy necessary to form such wrinkles, while in the case of graphene domains on Ir the adhesion or breaking of bonds between the graphene and the Ir substrate during wrinkle formation requires significant thermal activation. Once wrinkles exist, for both the tablecloth and the graphene, the wrinkles simply keep growing during further compression. For such strain relaxation mechanism to work, it is necessary for the graphene to be able to glide over the surface at little, but finite, energetic expense, which is possible due to the incommensurability of graphene on Ir. If the wrinkled layer is stretched out again, first the compressive stress in the flat areas is relieved due to coherent expansion. In the case of graphene on the expanding Ir lattice, this can even occur without gliding. Ultimately, after the wrinkles have been stretched out, tensile stress must form, just as there is no elastic relief mechanism for tensile stress in a flat table cloth.

Not surprisingly, our observation of a hysteretic evolution of the lattice parameter has not been observed in molecular dynamics simulations for the same system[39] without taking wrinkling into account. The hysteretic behavior of the graphene lattice parameter is thus intimately linked to the hysteresis in wrinkling and thus free-standing graphene layers will neither show wrinkling nor a hysteretic behavior.[40] In accordance with our previous elastic model,[23] we expect the interplay between strain and wrinkles for graphene on Ir(111) to be similar for

dx.doi.org/10.1021/nl203530t | Nano Lett. 2012, 12, 678–682

graphene grown by CVD at high temperatures on any substrate. During cooling, depending on the balance between binding to the substrate, bending, and elasticity, the thermally induced elastic strain will be partly accommodated by wrinkles, and partly be left as strain within the graphene. The use of thin epitaxial metal films on substrates with small thermal expansion coefficients are thus expected to reduce thermally induced strain and suppress wrinkling.[12] Strong binding also diminishes wrinkling and favors residual strain in graphene.

Since the wrinkle formation can be reversed by heating, we conclude that after releasing a strained and wrinkled graphene film from the substrate, both the compressive strain and the wrinkles can be relieved without leaving stress-induced morphological defects behind. This implies that as long as graphene layers are not fixed to another support prior to releasing the graphene off the substrate, it might be possible to transfer a completely relaxed and wrinkle-free graphene layer to a new support, even if the graphene is strained and wrinkled on the substrate.

AUTHOR INFORMATION

Corresponding Author

*E-mail: horn-von-hoegen@uni-due.de.

Present Addresses

[⊥]National Center for Electron Microscopy, Lawrence Berkeley National Laboratory, Berkeley, CA 94720, United States.

[¶]Departments of Physics and Electrical Engineering, Columbia University, 538 West 120th Street, New York, NY 10027, United States.

ACKNOWLEDGMENTS

This work was supported by the German Research Foundation through SFB616 "Energy Dissipation at Surfaces".

REFERENCES

(1) Liao, L.; Lin, Y.-C.; Bao, M.; Cheng, R.; Bai, J.; Liu, Y.; Qu, Y.; Wang, K. L.; Huang, Y.; Duan, X. *Nature* **2010**, *467*, 305.

(2) Xia, F.; Mueller, T.; Lin, Y.-M.; Valdes-Garcia, A.; Avouris, P. *Nat. Nanotech.* **2009**, *4*, 839.

(3) Lin, Y.-M.; Dimitrakopoulos, C.; Jenkins, K. A.; Farmer, D. B.; Chiu, H.-Y.; Grill, A.; Avouris, Ph. *Science* **2010**, *327*, 662.

(4) Kim, K. S.; Zhao, Y.; Jang, H.; Lee, S. Y.; Kim, J. M.; Kim, K. S.; Ahn, J.-H.; Kim, P.; Choi, J.-Y.; Hong, B. H. *Nature* **2009**, *457*, 706.

(5) Emtsev, K. V.; Bostwick, A.; Horn, K.; Jobst, J.; Kellogg, G. L.; Ley, L.; McChesney, J. L.; Ohta, T.; Reshanov, S. A.; Röhrl, J.; Rotenberg, E.; Schmid, A. K.; Waldmann, D.; Weber, H. B.; Seyller, T. *Nat. Mater.* **2009**, *8*, 203.

(6) Hass, J.; Feng, R.; Li, T.; Li, X.; Zong, Z.; de Heer, W. A.; First, P. N.; Conrad, E. H.; Jeffrey, C. A.; Berger, C. *Appl. Phys. Lett.* **2006**, *89*, 143106.

(7) Li, X.; Cai, W.; An, J.; Kim, S.; Nah, D.; Yang, J.; Piner, R.; Velamakanni, A.; Jung, I.; Tutuc, E.; Banerjee, S. K.; Colombo, L.; Ruoff, R. S. *Science* **2009**, *324*, 1312.

(8) Hu, B.; Ago, H.; Ito, Y.; Kawahara, K.; Tsuji, M.; Magome, E.; Sumitani, K.; Mizuta, N.; Ikeda, K.; Mizuno, S. *Carbon* **2012**, *50*, 57.

(9) Iwasaki, T.; Park, H. J.; Konuma, M.; Lee, D. S.; Smet, H. J.; Starke, U. *Nano Lett.* **2011**, *11*, 79.

(10) Reddy, K. M.; Gledhill, A. D.; Hu Chen, C; Drexler, J. M.; Padture, N. P. *Appl. Phys. Lett.* **2011**, *98*, 113117.

(11) Sutter, P. W.; Albrecht, P. M.; Sutter, E. A. *Appl. Phys. Lett.* **2010**, *97*, 213101.

(12) Vo-Van, C.; Kimouche, A.; Reserbat-Plantey, A.; Fruchart, O.; Bayle-Guillemaud, P.; Bendiab, N.; Coraux, J. *Appl. Phys. Lett.* **2011**, *98*, 181903.

(13) Sutter, E.; Acharya, D. P.; Sadowski, J. T.; Sutter, P. *Appl. Phys. Lett.* **2009**, *94*, 133101.

(14) Sutter, P.; Hybertsen, M. S.; Sadowski, J. T.; Sutter, E. *Nano Lett.* **2009**, *9*, 2654.

(15) Sutter, P.; Sadowski, J. T.; Sutter, E. A. *J. Am. Chem. Soc.* **2010**, *132*, 8175.

(16) Coraux, J.; N'Diaye, A. T.; Busse, C.; Michely, T. *Nano Lett.* **2008**, *8*, 565.

(17) Loginova, E.; Nie, S.; Thürmer, K.; Bartelt, N. C.; McCarty, K. F. *Phys. Rev. B* **2009**, *80*, 085430.

(18) Hattab, H.; N'Diaye, A. T.; Wall, D.; Jnawali, G.; Coraux, J.; Busse, C.; van Gastel, R.; Poelsema, B.; Michely, T.; Meyer zu Heringdorf, F.-J.; Horn-von Hoegen, M. *Appl. Phys. Lett.* **2011**, *98*, 141903.

(19) van Gastel, R.; N'Diaye, A. T.; Wall, D.; Coraux, J.; Busse, C.; Buckanie, N. M.; Meyer zu Heringdorf, F.-J.; Horn-von Hoegen, M.; Michely, T.; Poelsema, B. *Appl. Phys. Lett.* **2009**, *95*, 121901.

(20) Biedermann, L. B.; Bolen, M. L.; Capano, M. A.; Zemlyanov, D.; Reifenberger, R. G. *Phys. Rev. B* **2009**, *79*, 125411.

(21) Cambaza, Z. G.; Yushinb, G.; Osswalda, S.; Mochalina, V.; Gogotsi, Y. *Carbon* **2008**, *46*, 841.

(22) Chae, S. J.; Günes, F.; Kim, K. K.; Kim, E. S.; Han, G. H.; Kim, S. M.; Shin, H.-J.; Yoon, S.-M.; Choi, J.-Y.; Park, M. H.; Yang, C. W.; Pribat, D.; Lee, Y. H. *Adv. Mater.* **2009**, *21*, 2328.

(23) N'Diaye, A. T.; van Gastel, R.; Martínez-Galera, A.; Coraux, J.; Hattab, H.; Wall, D.; Meyer zu Heringdorf, F.-J.; Horn-von Hoegen, M.; Gómez-Rodríguez, J. M.; Poelsema, B.; Busse, C.; Michely, T. *New J. Phys.* **2009**, *11*, 113056.

(24) Obraztsov, A. N.; Obraztsova, A. V.; Tyurnina, E. A; Zolotukhin, A. A. *Carbon* **2007**, *45*, 2017.

(25) Sun, G. F.; Jia, J. F.; Xue, Q. K.; Li, L. *Nanotechnology* **2009**, *20*, 355701.

(26) Chen, S.; Moore, A. L.; Cai, W.; Suk, J. W.; An, J.; Mishra, C.; Amos, C.; Magnuson, C. W.; Kang, J.; Li Shi.; Ruoff, R. S. *ACS Nano* **2011**, *5*, 321.

(27) Pereira, V. M.; Castro Neto, A. H.; Liang, H. Y.; Mahadevan, L. *Phys. Rev. Lett.* **2010**, *105*, 156603.

(28) Starodub, E.; Bartelt, N. C.; McCarty, K. F. *J. Phys. Chem. C* **2010**, *114*, 5134.

(29) Horn-von Hoegen, M. *Z. Kristallogr.* **1999**, *214*, 591.

(30) Horn-von Hoegen, M. *Z. Kristallogr.* **1999**, *214*, 684.

(31) Scheithauer, U.; Meyer, G.; Henzler, M. *Surf. Sci.* **1986**, *178*, 441.

(32) N'Diaye, Alpha T.; Coraux, J.; Plasa, T. N.; Busse, C.; Michely, T. *New J. Phys.* **2008**, *10*, 043033.

(33) Coraux, J.; N'Diaye, A. T.; Engler, M.; Busse, C.; Wall, D.; Buckanie, N.; Meyer zu Heringdorf, F.-J.; van Gastel, R.; Poelsema, B.; Michely, T. *New J. Phys.* **2009**, *11*, 023006.

(34) Creath, K.; Wyant, J. *Optical Shop Testing 16: Moiré and Fringe Projection Techniques*; Wiley: New York, 1992, 653.

(35) Group III: Condensed Matter. In *Landolt-Börnstein Numerical Data and Functional Relationships in Science and Technology - new Series*; Eckerlin, P., Kandler, H., Eds.; Springer: Berlin, 1971; Vol. *6*.

(36) Halvorson, J. J.; Wimber, R. T. *J. Appl. Phys.* **1972**, *43*, 2519.

(37) Singh, H. P. *Acta Cryst.* **1968**, *A24*, 469.

(38) *Physics Handbook*; Dwight, E. G., Ed.; American Institute of Physics: 1972; Vol. *1*.

(39) Pozzo, M.; Alfè, D.; Lacovig, P.; Hofmann, P.; Lizzit, S.; Baraldi, A. *Phys. Rev. Lett.* **2011**, *106*, 135501.

(40) Zakharchenko, K. V.; Katsnelson, M. I.; Fasolino, A. *Phys. Rev. Lett.* **2009**, *102*, 046808.